



Fermi National Accelerator Laboratory

FERMILAB-Pub-93/234-E

CDF

Measurement of the Antiproton-Proton Total Cross Section at $\sqrt{s} = 546$ and 1800 GeV

**F. Abe et al
The CDF Collaboration**

*Fermi National Accelerator Laboratory
P.O. Box 500, Batavia, Illinois 60510*

August 1993

Submitted to *Physical Review D*

Disclaimer

This report was prepared as an account of work sponsored by an agency of the United States Government. Neither the United States Government nor any agency thereof, nor any of their employees, makes any warranty, express or implied, or assumes any legal liability or responsibility for the accuracy, completeness, or usefulness of any information, apparatus, product, or process disclosed, or represents that its use would not infringe privately owned rights. Reference herein to any specific commercial product, process, or service by trade name, trademark, manufacturer, or otherwise, does not necessarily constitute or imply its endorsement, recommendation, or favoring by the United States Government or any agency thereof. The views and opinions of authors expressed herein do not necessarily state or reflect those of the United States Government or any agency thereof.

Measurement of the Antiproton-Proton Total Cross Section at $\sqrt{s}=546$ and 1800 GeV

F. Abe,⁽¹²⁾ M. Albrow,⁽⁶⁾ D. Amidei,⁽¹⁵⁾ C. Anway-Wiese,⁽³⁾ G. Apollinari,⁽²³⁾ M. Atac,⁽⁶⁾
P. Auchincloss,⁽²²⁾ P. Azzi,⁽¹⁷⁾ N. Bacchetta,⁽¹⁶⁾ A. R. Baden,⁽⁸⁾ W. Badgett,⁽¹⁵⁾
M. W. Bailey,⁽²¹⁾ A. Bamberger,^(6,*) P. de Barbaro,⁽²²⁾ A. Barbaro-Galtieri,⁽¹³⁾
V. E. Barnes,⁽²¹⁾ B. A. Barnett,⁽¹¹⁾ G. Bauer,⁽¹⁴⁾ T. Baumann,⁽⁸⁾ F. Bedeschi,⁽²⁰⁾
S. Behrends,⁽²⁾ S. Belforte,⁽²⁰⁾ G. Bellettini,⁽²⁰⁾ J. Bellinger,⁽²⁸⁾ D. Benjamin,⁽²⁷⁾
J. Benlloch,⁽¹⁴⁾ J. Bensinger,⁽²⁾ A. Beretvas,⁽⁶⁾ J. P. Berge,⁽⁶⁾ S. Bertolucci,⁽⁷⁾ K. Biery,⁽¹⁰⁾
S. Bhadra,⁽⁹⁾ M. Binkley,⁽⁶⁾ D. Bisello,⁽¹⁷⁾ R. Blair,⁽¹⁾ C. Blocker,⁽²⁾ A. Bodek,⁽²²⁾
V. Bolognesi,⁽²⁰⁾ A. W. Booth,⁽⁶⁾ C. Boswell,⁽¹¹⁾ G. Brandenburg,⁽⁸⁾ D. Brown,⁽⁸⁾
E. Buckley-Geer,⁽⁶⁾ H. S. Budd,⁽²²⁾ G. Busetto,⁽¹⁷⁾ A. Byon-Wagner,⁽⁶⁾ K. L. Byrum,⁽¹⁾
C. Campagnari,⁽⁶⁾ M. Campbell,⁽¹⁵⁾ A. Caner,⁽⁶⁾ R. Carey,⁽⁸⁾ W. Carithers,⁽¹³⁾
D. Carlsmith,⁽²⁸⁾ J. T. Carroll,⁽⁶⁾ R. Cashmore,^(6,*) A. Castro,⁽¹⁷⁾ Y. Cen,⁽¹⁸⁾ F. Cervelli,⁽²⁰⁾
K. Chadwick,⁽⁶⁾ J. Chapman,⁽¹⁵⁾ T. J. Chapin,⁽²³⁾ G. Chiarelli,⁽⁷⁾ W. Chinowsky,⁽¹³⁾
S. Cihangir,⁽⁶⁾ A. G. Clark,⁽⁶⁾ M. Cobal,⁽²⁰⁾ D. Connor,⁽¹⁸⁾ M. Contreras,⁽⁴⁾
J. Cooper,⁽⁶⁾ M. Cordelli,⁽⁷⁾ D. Crane,⁽⁶⁾ J. D. Cunningham,⁽²⁾ C. Day,⁽⁶⁾ F. DeJongh,⁽⁶⁾
S. Dell'Agnello,⁽²⁰⁾ M. Dell'Orso,⁽²⁰⁾ L. Demortier,⁽²³⁾ B. Denby,⁽⁶⁾ P. F. Derwent,⁽¹⁵⁾
T. Devlin,⁽²⁴⁾ M. Dickson,⁽²²⁾ R. B. Drucker,⁽¹³⁾ A. Dunn,⁽¹⁵⁾ K. Einsweiler,⁽¹³⁾ J. E. Elias,⁽⁶⁾
R. Ely,⁽¹³⁾ S. Eno,⁽⁴⁾ S. Errede,⁽⁹⁾ A. Etchegoyen,^(6,*) B. Farhat,⁽¹⁴⁾ M. Frautschi,⁽¹⁶⁾
G. J. Feldman,⁽⁸⁾ B. Flaughner,⁽⁶⁾ G. W. Foster,⁽⁶⁾ M. Franklin,⁽⁸⁾ J. Freeman,⁽⁶⁾
T. Fuess,⁽⁶⁾ Y. Fukui,⁽¹²⁾ A. F. Garfinkel,⁽²¹⁾ A. Gauthier,⁽⁹⁾ S. Geer,⁽⁶⁾ D. W. Gerdes,⁽¹⁵⁾
P. Giannetti,⁽²⁰⁾ N. Giokaris,⁽²³⁾ P. Giromini,⁽⁷⁾ L. Gladney,⁽¹⁸⁾ M. Gold,⁽¹⁶⁾ J. Gonzalez,⁽¹⁸⁾
K. Goulianos,⁽²³⁾ H. Grassmann,⁽¹⁷⁾ G. M. Grieco,⁽²⁰⁾ R. Grindley,⁽¹⁰⁾ C. Grosso-Pilcher,⁽⁴⁾
J. Grunhaus,⁽²³⁾ C. Haber,⁽¹³⁾ S. R. Hahn,⁽⁶⁾ R. Handler,⁽²⁸⁾ K. Hara,⁽²⁶⁾ B. Harral,⁽¹⁸⁾
R. M. Harris,⁽⁶⁾ S. A. Hauger,⁽⁵⁾ J. Hauser,⁽³⁾ C. Hawk,⁽²⁴⁾ T. Hessing,⁽²⁵⁾ R. Hollebeek,⁽¹⁸⁾
L. Holloway,⁽⁹⁾ A. Hölscher,⁽¹⁰⁾ S. Hong,⁽¹⁵⁾ G. Houk,⁽¹⁸⁾ P. Hu,⁽¹⁹⁾ B. Hubbard,⁽¹³⁾
B. T. Huffman,⁽¹⁹⁾ R. Hughes,⁽²²⁾ P. Hurst,⁽⁸⁾ J. Huth,⁽⁶⁾ J. Hylen,⁽⁶⁾ M. Incagli,⁽²⁰⁾
T. Ino,⁽²⁶⁾ H. Iso,⁽²⁶⁾ C. P. Jessop,⁽⁸⁾ R. P. Johnson,⁽⁶⁾ U. Joshi,⁽⁶⁾ R. W. Kadel,⁽¹³⁾
T. Kamon,⁽²⁵⁾ S. Kanda,⁽²⁶⁾ D. A. Kardelis,⁽⁹⁾ I. Karliner,⁽⁹⁾ E. Kearns,⁽⁸⁾ L. Keeble,⁽²⁵⁾
R. Kephart,⁽⁶⁾ P. Kesten,⁽²⁾ R. M. Keup,⁽⁹⁾ H. Keutelian,⁽⁶⁾ D. Kim,⁽⁶⁾ S. B. Kim,⁽¹⁵⁾
S. H. Kim,⁽²⁶⁾ Y. K. Kim,⁽¹³⁾ L. Kirsch,⁽²⁾ K. Kondo,⁽²⁶⁾ J. Konigsberg,⁽⁸⁾ K. Kordas,⁽¹⁰⁾ E.
Kovacs,⁽⁶⁾ M. Krasberg,⁽¹⁵⁾ S. E. Kuhlmann,⁽¹⁾ E. Kuns,⁽²⁴⁾ A. T. Laasanen,⁽²¹⁾ S. Lammel,⁽³⁾
J. I. Lamoureux,⁽²⁸⁾ S. Leone,⁽²⁰⁾ J. D. Lewis,⁽⁶⁾ W. Li,⁽¹⁾ P. Limon,⁽⁶⁾ M. Lindgren,⁽³⁾
T. M. Liss,⁽⁹⁾ N. Lockyer,⁽¹⁸⁾ M. Loretì,⁽¹⁷⁾ E. H. Low,⁽¹⁸⁾ D. Lucchesi,⁽²⁰⁾ C. B. Luchini,⁽⁹⁾
P. Lukens,⁽⁶⁾ P. Maas,⁽²⁸⁾ K. Maeshima,⁽⁶⁾ M. Mangano,⁽²⁰⁾ J. P. Marriner,⁽⁶⁾ M. Mariotti,⁽²⁰⁾
R. Markeloff,⁽²⁸⁾ L. A. Markosky,⁽²⁸⁾ J. A. J. Matthews,⁽¹⁶⁾ R. Mattingly,⁽²⁾ P. McIntyre,⁽²⁵⁾
A. Menzione,⁽²⁰⁾ E. Meschi,⁽²⁰⁾ T. Meyer,⁽²⁵⁾ S. Mikamo,⁽¹²⁾ M. Miller,⁽⁴⁾ T. Mimashi,⁽²⁶⁾
S. Miscetti,⁽⁷⁾ M. Mishina,⁽¹²⁾ S. Miyashita,⁽²⁶⁾ Y. Morita,⁽²⁶⁾ S. Moulding,⁽²³⁾ J.
Mueller,⁽²⁴⁾ A. Mukherjee,⁽⁶⁾ T. Muller,⁽³⁾ L. F. Nakae,⁽²⁾ I. Nakano,⁽²⁶⁾ C. Nelson,⁽⁶⁾
D. Neuberger,⁽³⁾ C. Newman-Holmes,⁽⁶⁾ J. S. T. Ng,⁽⁸⁾ M. Ninomiya,⁽²⁶⁾ L. Nodulman,⁽¹⁾

Submitted to Physical Review D, August 3, 1993

S. Ogawa,⁽²⁶⁾ R. Paoletti,⁽²⁰⁾ V. Papadimitriou,⁽⁶⁾ A. Para,⁽⁶⁾ E. Pare,⁽⁸⁾ S. Park,⁽⁶⁾
 J. Patrick,⁽⁶⁾ G. Pauletta,⁽²⁰⁾ L. Pescara,⁽¹⁷⁾ T. J. Phillips,⁽⁵⁾ A. G. Piacentino,⁽²⁰⁾
 R. Plunkett,⁽⁶⁾ L. Pondrom,⁽²⁸⁾ J. Proudfoot,⁽¹⁾ F. Ptohos,⁽⁸⁾ G. Punzi,⁽²⁰⁾ D. Quarrie,⁽⁶⁾
 K. Ragan,⁽¹⁰⁾ G. Redlinger,⁽⁴⁾ J. Rhoades,⁽²⁸⁾ M. Roach,⁽²⁷⁾ F. Rimondi,^(6,*) L. Ristori,⁽²⁰⁾
 W. J. Robertson,⁽⁵⁾ T. Rodrigo,⁽⁶⁾ T. Rohaly,⁽¹⁸⁾ A. Roodman,⁽⁴⁾ W. K. Sakumoto,⁽²²⁾
 A. Sansoni,⁽⁷⁾ R. D. Sard,⁽⁹⁾ A. Savoy-Navarro,⁽⁶⁾ V. Scarpine,⁽⁹⁾ P. Schlabach,⁽⁸⁾,
 E. E. Schmidt,⁽⁶⁾ O. Schneider,⁽¹³⁾ M. H. Schub,⁽²¹⁾ R. Schwitters,⁽⁸⁾ G. Sciacca,⁽²⁰⁾
 A. Scribano,⁽²⁰⁾ S. Segler,⁽⁶⁾ S. Seidel,⁽¹⁶⁾ Y. Seiya,⁽²⁶⁾ G. Sganos,⁽¹⁰⁾ N. M. Shaw,⁽²¹⁾
 M. Sheaff,⁽²⁸⁾ M. Shochet,⁽⁴⁾ J. Siegrist,⁽¹³⁾ A. Sill,⁽²²⁾ P. Sinervo,⁽¹⁰⁾ J. Skarha,⁽¹¹⁾
 K. Sliwa,⁽²⁷⁾ D. A. Smith,⁽²⁰⁾ F. D. Snider,⁽¹¹⁾ L. Song,⁽⁶⁾ T. Song,⁽¹⁵⁾ M. Spahn,⁽¹³⁾
 P. Sphicas,⁽¹⁴⁾ A. Spies,⁽¹¹⁾ R. St. Denis,⁽⁸⁾ L. Stanco,⁽¹⁷⁾ A. Stefanini,⁽²⁰⁾ G. Sullivan,⁽⁴⁾
 K. Sumorok,⁽¹⁴⁾ R. L. Swartz, Jr.,⁽⁹⁾ M. Takano,⁽²⁶⁾ K. Takikawa,⁽²⁶⁾ S. Tarem,⁽²⁾
 F. Tartarelli,⁽²⁰⁾ S. Tether,⁽¹⁴⁾ D. Theriot,⁽⁶⁾ M. Timko,⁽²⁷⁾ P. Tipton,⁽²²⁾ S. Tkaczyk,⁽⁶⁾
 A. Tollestrup,⁽⁶⁾ J. Tonnison,⁽²¹⁾ W. Trischuk,⁽⁸⁾ Y. Tsay,⁽⁴⁾ J. Tseng,⁽¹¹⁾ N. Turini,⁽²⁰⁾
 F. Ukegawa,⁽²⁶⁾ D. Underwood,⁽¹⁾ S. Vejcek, III,⁽¹⁵⁾ R. Vidal,⁽⁶⁾ R. G. Wagner,⁽¹⁾
 R. L. Wagner,⁽⁶⁾ N. Wainer,⁽⁶⁾ R. C. Walker,⁽²²⁾ J. Walsh,⁽¹⁸⁾ A. Warburton,⁽¹⁰⁾
 G. Watts,⁽²²⁾ T. Watts,⁽²⁴⁾ R. Webb,⁽²⁵⁾ C. Wendt,⁽²⁸⁾ H. Wenzel,⁽²⁰⁾ W. C. Wester, III,⁽¹³⁾
 T. Westhusing,⁽⁹⁾ S. N. White,⁽²³⁾ A. B. Wicklund,⁽¹⁾ E. Wicklund,⁽⁶⁾ H. H. Williams,⁽¹⁸⁾
 B. L. Winer,⁽²²⁾ J. Wolinski,⁽²⁵⁾ D. Y. Wu,⁽¹⁵⁾ X. Wu,⁽²⁰⁾ J. Wyss,⁽¹⁷⁾ A. Yagil,⁽⁶⁾
 K. Yasuoka,⁽²⁶⁾ Y. Ye,⁽¹⁰⁾ G. P. Yeh,⁽⁶⁾ J. Yoh,⁽⁶⁾ M. Yokoyama,⁽²⁶⁾ J. C. Yun,⁽⁶⁾
 A. Zanetti,⁽²⁰⁾ F. Zetti,⁽²⁰⁾ S. Zhang,⁽¹⁵⁾ W. Zhang,⁽¹⁸⁾ S. Zucchelli,^(6,*)

(CDF Collaboration)

- (1) Argonne National Laboratory, Argonne, Illinois 60439
- (2) Brandeis University, Waltham, Massachusetts 02254
- (3) University of California at Los Angeles, Los Angeles, California 90024
- (4) University of Chicago, Chicago, Illinois 60637
- (5) Duke University, Durham, North Carolina 27706
- (6) Fermi National Accelerator Laboratory, Batavia, Illinois 60510
- (7) Laboratori Nazionali di Frascati, Istituto Nazionale di Fisica Nucleare, Frascati, Italy
- (8) Harvard University, Cambridge, Massachusetts 02138
- (9) University of Illinois, Urbana, Illinois 61801
- (10) Institute of Particle Physics, McGill University, Montreal, and University of Toronto, Toronto, Canada
- (11) The Johns Hopkins University, Baltimore, Maryland 21218
- (12) National Laboratory for High Energy Physics (KEK), Japan
- (13) Lawrence Berkeley Laboratory, Berkeley, California 94720
- (14) Massachusetts Institute of Technology, Cambridge, Massachusetts 02139
- (15) University of Michigan, Ann Arbor, Michigan 48109
- (16) University of New Mexico, Albuquerque, New Mexico 87131

* Visitor

- (17) *Università di Padova, Istituto Nazionale di Fisica Nucleare, Sezione di Padova, I-35131 Padova, Italy*
- (18) *University of Pennsylvania, Philadelphia, Pennsylvania 19104*
- (19) *University of Pittsburgh, Pittsburgh, Pennsylvania 15260*
- (20) *Istituto Nazionale di Fisica Nucleare, University and Scuola Normale Superiore of Pisa, I-56100 Pisa, Italy*
- (21) *Purdue University, West Lafayette, Indiana 47907*
- (22) *University of Rochester, Rochester, New York 15627*
- (23) *Rockefeller University, New York, New York 10021*
- (24) *Rutgers University, Piscataway, New Jersey 08854*
- (25) *Texas A&M University, College Station, Texas 77843*
- (26) *University of Tsukuba, Tsukuba, Ibaraki 305, Japan*
- (27) *Tufts University, Medford, Massachusetts 02155*
- (28) *University of Wisconsin, Madison, Wisconsin 53706*

Abstract

We report a measurement of the proton-antiproton total cross section, σ_T , at c.m.s. energies $\sqrt{s} = 546$ and 1800 GeV. Using the luminosity independent method, we find $\sigma_T = 61.26 \pm 0.93$ mb at $\sqrt{s} = 546$ GeV and 80.03 ± 2.24 mb at $\sqrt{s} = 1800$ GeV. In this energy range, the ratio σ_{el}/σ_T increases from 0.210 ± 0.002 to 0.246 ± 0.004 .

PACS numbers: 13.85.Lg, 12.40.Gg, 12.40.Pp

We have measured the total proton-antiproton cross section at the Fermilab Tevatron Collider at c.m.s. energies $\sqrt{s} = 546$ and 1800 GeV using the luminosity independent method [1, 2]. This method is based on the simultaneous measurement of the elastic scattering differential cross section at low four-momentum transfer-squared (t) and the total inelastic rate. The total cross section is the sum of the elastic and inelastic rates divided by the machine luminosity L :

$$\sigma_T = \frac{1}{L} \cdot (R_{el} + R_{in}) \quad (1)$$

The optical theorem relates the total cross section to the imaginary part of the forward

elastic scattering rate,

$$\sigma_T^2 = \frac{16\pi(\hbar c)^2}{1 + \rho^2} \cdot \frac{1}{L} \cdot dR_{el}/dt|_{t=0} \quad (2)$$

where ρ is the ratio of the real to imaginary part of the forward elastic scattering amplitude. Dividing (2) by (1) yields

$$\sigma_T = \frac{16\pi(\hbar c)^2}{1 + \rho^2} \cdot \frac{dR_{el}/dt|_{t=0}}{R_{el} + R_{in}} \quad (3)$$

At present, only this method provides a precise measurement of the Tevatron luminosity and of the total cross section.

I. EXPERIMENTAL METHOD

The data for the total cross section measurement were collected in short dedicated runs during the 1988-1989 data taking period of CDF. At each energy, the machine optics was specially tuned to enable detection of low- t elastic scattering events. The elastic scattering and inelastic rates were measured simultaneously (the inelastic trigger was conveniently prescaled).

The elastic scattering measurement is reported in the preceding paper [3]. The apparatus used to measure the inelastic rate is shown in Fig. 1. The region of polar angles $3.5^\circ < \theta < 176.5^\circ$ ($|\eta| < 3.5$) was covered by the VTPC [4], a system of eight time projection chambers around the beam pipe, mounted end-to-end along the beam direction (z -axis). These chambers provided accurate event vertex and tracking information. They employed 3072 sense wires and 3072 pads for the measurement of

track coordinates projected onto the r - z and r - ϕ planes, where r is the radial distance from the beam line. The active region of the chambers was 2.8 m along the beam direction, covering well the interaction region ($\sigma_z \simeq 30$ cm), and extended from $r=6.8$ cm to $r=21$ cm. The VTPC provided single-hit precision of 200-500 μm and two-track resolution of 6 mm in the R - z plane.

Two identical forward telescopes (S4+FTB and S5+FTF), added to the CDF detector for these special runs, were placed symmetrically on the west (outgoing \bar{p}) and east (outgoing p) sides of the interaction region. The detectors FTB (FTF) covered the polar angles $0.45^\circ < \theta < 2.56^\circ$ ($179.55^\circ > \theta > 177.44^\circ$), corresponding to $3.8 < |\eta| < 5.5$. Each FTB/FTF telescope consisted of four drift chambers separated by 25 cm along the z -axis[5]. Each chamber contained a front section, which measured the (horizontal) x -coordinate in four parallel drift cells (4 cm wide by 36 cm long) on each side of the beam-pipe, and an identical back section with sense wires rotated by 90° for measuring the (vertical) y -coordinate. In addition, in every drift cell, the coordinate perpendicular to the drift direction was measured with a delay line placed close to the sense wire, providing in most cases unambiguous reconstruction of space points. The drift time measurement provided single-hit accuracy of 700 μm and two-track resolution of 4.0 mm. The single-hit accuracy of the delay line was 2.0 cm and the two-track resolution about 12 cm.

The S4 and S5 telescopes extended the polar angle coverage down to $\theta \simeq 0.14^\circ$ and $\theta \simeq 179.86^\circ$ ($|\eta| \simeq 6.7$), respectively. Each telescope contained two drift chambers separated by 1 m along the z -axis. Each chamber had two sections, one above and one below the beam line. These sections were inserted in a beam pipe with variable aperture. When stable beam conditions were reached, the two sections were pushed

close to the beam forming a $7.0 \text{ cm} \times 7.0 \text{ cm}$ square with a 1.2 cm radius hole around the beam line. Each section had four drift cells sampling four times the y-coordinate of a track along the beam direction. A delay line placed close to the sense wires measured the x-coordinate. The drift measurement provided single-hit accuracy of $200 \text{ } \mu\text{m}$ and two-track resolution of 4 mm ; the single-hit resolution of the delay line was $420 \text{ } \mu\text{m}$ and the two-track resolution about 2 cm . Each S4 and S5 chamber section was backed by a trigger counter. In addition, two scintillator hodoscopes (BBCW and BBCE [4]) were located behind the S4 and S5 telescopes, covering the polar angles $0.32^\circ < \theta < 4.47^\circ$ and $179.68^\circ > \theta > 175.53^\circ$.

Data were taken with two inelastic triggers, making use of BBCW, BBCE, the counters of S4, S5 and the counters of S1, S2 on the outgoing \bar{p} side of the elastic spectrometer [3]:

(a) Inelastic trigger ($W \bullet E$): the condition $[W=(\text{BBCW}+S4) \bullet E=(\text{BBCE}+S5)]$ was fulfilled by events with at least one particle at $3.2 < |\eta| < 6.7$ on both the west and east sides of the interaction region; this trigger detected almost all inelastic (non-diffractive) events.

(b) Inelastic trigger ($\bar{p} \bullet E$): the requirement $[(S1 \bullet S2) \bullet E]$ was fulfilled by the ~~proton~~ single diffraction dissociation interactions that might escape the ($W \bullet E$) trigger. The observed trigger rate was multiplied by two to account for the antiproton diffraction dissociation. This trigger was preferred to the traditional one-side-only trigger [2] to reduce the background contamination [6]. Proton dissociation events were chosen because of the excellent spectrometer momentum resolution for the recoil antiproton [7].

The analysis of the events collected by the ($\bar{p}\bullet E$) trigger is described in the preceding paper [7]; the following section describes only the analysis of the events collected by the ($W\bullet E$) trigger.

II. DATA REDUCTION

The data at $\sqrt{s}=546$ GeV were collected in one run with average luminosity $L \simeq 3.2 \cdot 10^{27} \text{ cm}^{-2}\cdot\text{sec}^{-1}$. The data at $\sqrt{s}=1800$ GeV were collected in two different runs with average luminosity $L \simeq 1.9 \cdot 10^{26} \text{ cm}^{-2}\cdot\text{sec}^{-1}$; the second run took place at the end of the $\sqrt{s}=546$ run.

In order to separate $\bar{p}p$ interactions from background, a first selection was made by rejecting events in which the time of flight analysis of the S4 (S5) counters showed early hits in time with the incoming proton (antiproton) beams (TOF FILTER). The S4 and S5 detectors, located 1.2 cm away from the beam axis, detected efficiently beam halo particles travelling inside the vacuum chamber; the TOF FILTER rejected most of the ($S4\bullet S5$) triggers due to random coincidences of these halo particles. In the $\sqrt{s}=546$ run and in the second $\sqrt{s}=1800$ run, a loose TOF FILTER was also applied by the level 3 trigger of CDF [8]. Events were also rejected if the VTPC detected particle showers originating upstream of the interaction region (VTPC FILTER). Table 1 summarizes the event flow through these filters. The above two filters removed most of the background at the expense of a small loss of good events. The event losses caused by the TOF FILTER ($< 1\%$) were evaluated by looking with the VTPC at the vertex z -distribution of a large sample of TOF rejected events. The losses due to the VTPC FILTER ($\leq 0.5\%$) were evaluated by looking with the forward telescopes at

the z -distribution of the rejected events. These losses are listed in Table 2.

When the level 3 trigger of CDF was used, about 10% of the inelastic triggers were lost in the hardware event-builder, a part of the CDF data acquisition system that, for every event, puts together the information coming from all detector components. The loss occurred at certain event record-sizes and was evaluated by interpolating the record-size distributions of the good $\bar{p}p$ interactions. This loss did not affect the short record-size elastic events or the first run at $\sqrt{s}=1800$, where as a check we used a software event-builder. The event-builder corrections are listed in Table 2.

In the remaining events, $\bar{p}p$ interactions are recognized by requiring a vertex and looking at its z -distribution. Details on the event vertex reconstruction procedure are given in Appendix A. Vertex z -distributions measured with all vertex detectors for the events at $\sqrt{s}=546$ are compared to our simulation in Fig 2. The excellent agreement between data and simulation is an indication of negligible background contamination and demonstrates that the detector resolution is well understood. Vertex z -distributions at $\sqrt{s}=1800$ are shown in Fig. 3; at this energy, there is a background contamination which appears in the tails of the distributions. For events in which the vertex was reconstructed by the VTPC, the data were fit with a gaussian form of width as determined by the simulation and a flat background (as expected for beam-gas interactions). For events reconstructed in the forward telescopes, the signal was also fit with a gaussian of width as determined by the simulation. The beam-gas background shape was determined by reconstructing with the forward telescopes the vertex of a small number of tagged background events. These background events were identified when the VTPC reconstructed only a secondary vertex more than four sigma away from the primary vertex determined by the timing information of the trigger counters

(the VTPC vertex z -distribution of these events is flat). The vertex analysis event flow is summarized in Table 3.

Corrections to the inelastic rate due the partial angular coverage of the trigger ($\simeq 1.0\%$) and to the requirement of a vertex to validate a good $\bar{p}p$ interaction ($\leq 0.5\%$), were evaluated using the simulation, which is described in Appendix B. These corrections are listed in Table 2. Finally, the inelastic rates were multiplied by the trigger prescaling factors, which are also listed in Table 2. The prescaling factors were determined with a full simulation of the trigger and the data acquisition system to account for dead time corrections. Using the data, we verified the calculated prescaling factors to within 1%, by studying the events (mostly background) which were contributed by more than one trigger at the same time. The quoted prescaling factor errors account for all uncertainties in the simulation inputs.

III. RESULTS

The corrected number of inelastic events contributed by the (W•E) trigger is listed in Table 4. The contribution of the (\bar{p} •E) inelastic trigger, as derived in [7], is also shown. The (W•E) and (\bar{p} •E) inelastic triggers share some high mass single diffraction events. To avoid double counting, we rejected those (\bar{p} •E) trigger events which also fired the W=BBCW+S4 counters. Fig. 4 shows the BBCW+S4 efficiency for rejecting single diffraction events as a function of the recoil momentum. By convoluting the BBCW+S4 rejection efficiency with the functional form that fits all single diffraction events [7], we obtained the number of events to be added to the inelastic rate, as listed in Table 4. As explained in detail in Appendix C, the inelastic (non-diffractive) contribution

($\simeq 0.4\%$) accepted by the ($\bar{p}\bullet E$) trigger was not added to the total inelastic rate, as it is already included in the simulation-calculated correction ($\simeq 1\%$) to the ($W\bullet E$) inelastic rate.

The results of the elastic scattering measurement, described in the preceding paper [3], are also listed for completeness in Table 4.

Substituting the rates listed in Table 4 into eq. (3), we obtain $(1+\rho^2)\cdot\sigma_T = 62.64\pm 0.95$ and 81.83 ± 2.29 mb at $\sqrt{s}=546$ and 1800 GeV, respectively. Assuming $\rho=0.15$, our results for the total cross section are 61.26 ± 0.93 mb at $\sqrt{s}=546$ and 80.03 ± 2.24 mb at $\sqrt{s}=1800$ GeV.

The elastic scattering cross sections are 12.87 ± 0.30 (19.70 ± 0.85) mb at $\sqrt{s}=546$ (1800) GeV.

From the elastic and total cross section values we derive the ratio $\sigma_{el}/\sigma_T = 0.210\pm 0.002$ (0.246 ± 0.004) at $\sqrt{s}=546$ (1800) GeV.

The single diffraction dissociation cross sections [7] are 7.89 ± 0.33 (9.46 ± 0.44) mb, and the inelastic cross sections are 48.39 ± 0.66 (60.33 ± 1.40) mb at $\sqrt{s}=546$ (1800) GeV.

Our results on σ_T and σ_{el}/σ_T are compared with other experiments ([9]-[16]) in Fig. 5.

CONCLUSIONS

We have measured the $\bar{p}p$ total cross section, σ_T , at $\sqrt{s}=546$ and 1800 GeV. At $\sqrt{s} = 546$ GeV, our measured value $\sigma_T=61.26\pm 0.93$ mb agrees with the UA4 result $\sigma_T=61.9\pm 1.5$ mb at the same energy, assuming in both cases the ratio of the real to imaginary part of the elastic scattering amplitude to be $\rho=0.15$. Our ratio $r = \sigma_{el}/\sigma_T=0.210\pm 0.002$ also agrees with the UA4 value $r=0.215\pm 0.005$.

At $\sqrt{s}=1800$ GeV, our result $\sigma_T=80.03\pm2.24$ mb is larger than the E710 result $\sigma_T=72.8\pm3.1$ mb [16]; our result $r = \sigma_{el}/\sigma_T=0.246\pm0.004$ agrees with the E710 value 0.23 ± 0.012 .

The continuing rise of r up to $\sqrt{s}=1800$ GeV is in qualitative agreement with the basic hypothesis of various optical models [17] in which the nucleon opacity increases with s , but the present energy is still far below the asymptotic regime of black-disk maximum absorption at which $r=0.5$. However, the central opaqueness of the nucleon, defined as $Imf(s,b)$ at $b=0$, where $f(s,b)$ is the elastic scattering amplitude in terms of the impact parameter b [18], has increased from 0.36 at the ISR [19] to 0.492 ± 0.008 at $\sqrt{s}=1800$ GeV and is close to the unitarity bound of 0.5 corresponding to complete absorption.

From $\sqrt{s_1}=546$ to $\sqrt{s_2}=1800$ [$s_2/s_1=10.9$, $\ln(s_2/s_1)=2.4$ and $\ln^2 s_2 - \ln^2 s_1=65.8$] the total cross section increases by 18.8 ± 2.5 mb. For comparison, a similar 17.6 ± 1.0 mb increase of σ_T is observed from the ISR energy $\sqrt{s_0}=52.8$ GeV to $\sqrt{s_1}=546$ GeV [but $s_1/s_0=107$, $\ln(s_1/s_0)=4.7$ and $\ln^2 s_1 - \ln^2 s_0=95.9$]. Interpreting the rise of σ_T observed in our energy range in the framework of models based on a supercritical pomeron [20], we derive a pomeron trajectory $\alpha(t)|_{t=0} = 1 + \epsilon$ with $\epsilon=0.112\pm0.013$.

In our energy range, while the inelastic cross section increases by a factor 1.25 ± 0.03 , the single diffraction cross section increases by 1.20 ± 0.07 .

ACKNOWLEDGEMENTS

We thank the Fermilab Accelerator Division for the construction and operation of the Tevatron and of the Antiproton Source. We wish to thank the Fermilab Computer Division, the technical staff of CDF and the collaborating Institutions for their con-

tribution to the construction and operation of CDF. The dedicated effort of the many technicians and engineers at Frascati and Rockefeller, who contributed to the design, construction and installation of the spectrometer and of the forward tracking vertex detectors, is warmly acknowledged; we especially thank M. Biagioli, G. Bisogni, A. Ceccarelli, M. DiVirgilio, G. Fontana, R. Heidecker, D. Humbert, E. Iacuesa, P. Locchi, A. Rutili, G. Sensolini, D. Scephanovich and M. Troiani. A very special thanks is due to our friends and colleagues R. Castaldi, C. Vannini and G. Sanguinetti, who made available to us most of the UA4 drift chambers (FTF and FTB), patiently introduced us to their reconstruction code and over several years have been helpful through many useful discussions. This work was supported by the Department of Energy, the National Science Foundation, the Istituto Nazionale di Fisica Nucleare and the Ministry of Science, Culture and Education of Japan.

APPENDIX A: EVENT VERTEX RECONSTRUCTION AND CHECKS ON DETECTOR EFFICIENCY

Fig. 6 shows z -distributions of the interaction vertex as reconstructed by the VTPC (z_{VTPC}), by the forward telescopes (z_{FT}), or by using the timing information of the trigger counters (z_{TOF}). When possible, the vertex was reconstructed using the VTPC. The VTPC system and the related vertex finding and track reconstruction algorithms have been described in previous publications [21, 22]. For events with only a few or no tracks in the VTPC, the vertex was reconstructed from tracks in the forward telescopes. In the FTF and FTB detectors, particles generate one x -drift and one y -drift hit at four z -locations. On both (x - z) and (y - z) planes, straight lines were drawn through

every first and last hit along the z -axis . A “track” required the presence of at least one hit in each of the two internal chambers within a region of 2 mm radius around the straight line. If more than one hit was available, the closest to the line was chosen. Every particle produced one track in the $(x-z)$ plane and one in the $(y-z)$ plane. Since one projection was enough to determine a vertex by determining its z -position at which $x(y)=0$, good detection efficiency was assured.

Tracks in the S4 and S5 detectors were reconstructed as in the elastic scattering spectrometer [3]. First, spatial points were determined in every chamber by requiring at least two out of the four drift hits. Tracks were then reconstructed by connecting by a straight line all spatial points of the two chambers covering the same polar angle at the different z -positions.

All tracks found by S4, FTF, FTB and S5 were projected to the z -coordinates (z_{track}) where $x=y=0$. To determine the vertex, only those z_{track} ’s values that were within three sigma from z_{TOF} were used, where sigma is the convolution of the error on z_{TOF} with the error on z_{track} . The z -position of the vertex was calculated by averaging the z_{track} ’s values weighted by their errors.

The efficiency of the forward telescopes was studied at length in several ways. The efficiency of the reconstruction code was tuned and checked with the simulation described in **Appendix B**. The forward telescopes reconstructed 99.8 % of all events with a z_{VTPC} vertex (**Fig. 7**). For the few events for which no tracks were reconstructed in the VTPC or in the forward telescope (see Table 5), a special reconstruction code was used requiring only three out of the four drift planes in the FTF and FTB telescopes. This procedure resulted in 0.2% additional events with flat vertex z -distribution.

Particular attention was paid to checking the efficiency of the trigger counters. The task

was straightforward for the S4 and S5 counters, which were close to the corresponding tracking chambers. We looked at events that triggered otherwise and, whenever a track segment was detected in one of the S4 or S5 chambers, we checked the pulse height of the corresponding counter. We found that, overall, the efficiency of all S4 and S5 counters was larger than 99.9%. The multi-counter BBC hodoscopes were located far from all tracking chambers, in a region where the majority of the particles in an event did not come from the interaction point but from secondary interactions in the beam pipe and leakage/albedo from the surrounding CDF calorimeters [4]. We found it hard to determine the efficiency of the BBC counters by using the data. However, the simulation showed that every single BBC counter was blasted by several particles per event and that, even under the unrealistic assumption that the BBC counters were 50% efficient, our inelastic and diffractive triggers would be fully efficient in all triggerable events. As shown in Table 5, the fractions of inelastic triggers contributed by different trigger counter combinations compare well with the prediction of the simulation in which the BBC counters were assumed fully efficient.

APPENDIX B: MONTE CARLO SIMULATION OF INELASTIC EVENTS

In our inelastic event simulation, at each energy we generate a system of mass $M = \sqrt{s}$. When generating single diffraction dissociation, M is the excited mass. The mass M (GeV) decays into n^* fictitious intermediate neutral objects with average multiplicity

$$\langle n^* \rangle = 2 + 0.13 \ln(M - m_p)^2 + 0.175 \ln^2(M - m_p)^2 \quad (4)$$

As described in Ref. [23], the multiplicity distribution of these objects is a gamma distribution,

$$\langle n^* \rangle P(n^*) = \frac{\mu^\mu}{\Gamma(\mu)} z^{\mu-1} e^{-\mu z}$$

where $z = n^* / \langle n^* \rangle$ and $\mu^{-1} = -0.104 + 0.058 \ln(M - m_p + 6.0)$. Each neutral object has equal probability of turning into a single neutral hadron or a pair of charged hadrons.

The rapidity (y) distribution of each hadron is generated in the interval $-\ln(M/m_p) = y_{\min} < y < y_{\max} = \ln(M/m_p)$. The distribution is flat for $|y| \leq y_{pt} = 0.4 \cdot y_{\max}$ and decreases linearly to zero from y_{pt} to $y_{\min(\max)}$. The transverse momentum p_t (GeV) of each hadron is generated with a probability

$$P(p_t) = \frac{p_t}{(1 + p_t/1.27)^{4+35.83/\ln(M/0.3)}}$$

This procedure defines the four-momentum (p_x, p_y, p_z, E) of each generated hadron. In our simulation, we balance the total momentum, conserve the energy \sqrt{s} and reproduce the measured $dn_{ch}/d\eta$ distributions at $\sqrt{s}=200, 546, 900$ and 1800 GeV as a function of the event multiplicity [22, 24]. The momentum is balanced by redefining the momentum of the i^{th} particle as

$$\begin{aligned} p'_{x,y} &= p_{x,y}^i - |p_{x,y}^i| \frac{\sum_{j=1}^n p_{x,y}^j}{\sum_{j=1}^n |p_{x,y}^j|} \\ p'_z &= p_z^i - |p_z^i|^\alpha \frac{\sum_{j=1}^n p_z^j}{\sum_{j=1}^n |p_z^j|^\alpha} \end{aligned}$$

We then define

$$P_z^{+(-)} = \sum_{j, p_z'^j > (<) 0} |p_z'^j|^\alpha, \quad E = \sum_{j=1}^n E'^j$$

and calculate in a few iterations the final longitudinal momenta

$$p_z''^i = p_z'^i \pm \frac{(M - E)}{2P_z^\pm} |p_z'^i|^\alpha.$$

The parameter α is an empirical function of the event total multiplicity n

$$\alpha = \begin{cases} 1.5 & \text{if } \frac{n}{\langle n \rangle} < 0.1 \\ 3.0 & \text{if } \frac{n}{\langle n \rangle} > 0.8 \\ 1.71 - 1.83 \frac{n}{\langle n \rangle} + 4.22 \left(\frac{n}{\langle n \rangle} \right)^2 & \text{otherwise} \end{cases}$$

where $\langle n \rangle = 1.5$ $\langle n^* \rangle$. When generating single diffraction events, we always assume $\alpha=3$.

In Table 5, fractions of inelastic triggers contributed by different trigger counter combinations and fractions of number of vertices detected by the different vertex detectors are compared with the simulation. The simulation is in good agreement with the data at $\sqrt{s}=546$, and with the data at $\sqrt{s}=1800$ after background subtraction.

Simulated **pseudo-rapidity** distributions as seen by the VTPC and by the forward telescopes are compared with the data at $\sqrt{s}=546$ in Fig. 8. The same comparison at $\sqrt{s}=1800$ is shown in Fig. 9; differences in the forward telescope are due to unsubtracted background contamination (see Table 3). The total number of measured tracks in all detectors compares well to the simulation at both energies (Fig. 10). However, the average track multiplicity in the data is about 10% larger than in the simulation,

eq.(4), which in turn generates an average charged multiplicity 10% larger than the value $\langle n_{ch} \rangle = -7.0 + 7.2 \cdot s^{0.127}$ measured by UA5 [25]. The average multiplicity in the simulation is the average between our finding and that of UA5, and work is in progress to extract from our data more accurate multiplicities and pseudorapidity distributions. As far as the total inelastic rate measurement is concerned, a $\pm 10\%$ change in the average multiplicity does not influence our extrapolated loss of inelastic events.

APPENDIX C : NON-DIFFRACTIVE CONTRIBUTION MEASURED BY THE INELASTIC ($\bar{p} \bullet E$) TRIGGER

As reported in our paper on single diffraction dissociation [7], 24483 ± 3926 events at $\sqrt{s}=546$ and 10276 ± 1712 at $\sqrt{s}=1800$ were accounted for as non-diffractive contribution to the ($\bar{p} \bullet E$) trigger at $x \geq 0.85$. By excluding events detected also by the ($W \bullet E$) trigger, 2024 ± 332 and 1311 ± 222 events are left at $\sqrt{s}=546$ and 1800 , respectively (see Table 4). At both energies, these events amount to $\simeq 0.4\%$ of the total inelastic rate, for which the simulation predicts a 1% loss.

At $\sqrt{s}=1800$, we simulated 70400 inelastic events; the antiproton recoil spectrometer was included in the simulation. We found that 337 events produced a ($\bar{p} \bullet E$) trigger and 102 also survived all our fiducial cuts [7]. Fig. 11 shows the leading particle momentum spectrum for these events. The momentum distribution extends to values larger than 900 GeV, clearly indicating that in inelastic events apparent production of particles at $x \simeq 1$ can be mistakenly achieved by reconstructing as high momentum recoils the products of secondary interactions wrongly assumed to come from the inter-

action point. With our fiducial cuts, we selected the simulated events with a particle at $x \simeq 1$.

These “recoils” were fit with the form (4) of [7], $d^2\sigma/dt dx = I \cdot e^{b't}(1-x)^\gamma$. In good agreement with [7], we found $b' = 5.3 \pm 1.6 \text{ GeV}^{-2}$ and $\gamma = 0.1 \pm 0.1$. The number of simulated events with a particle at $x \geq 0.85$, corrected by the spectrometer acceptance and normalized to the measured number of inelastic events, was 5510 ± 2120 (775 ± 246 when requiring the inelastic trigger veto). The simulation, without any special tuning at $x \simeq 1$, supports the functional form we used to fit the non-diffractive contribution in the data (an analogous x -distribution for the leading particle in inelastic events was also found in the UA5 simulation [26]). The simulation reproduces well the x and t behaviour observed in the inelastic (non-diffractive) data at $x \simeq 1$; within the large statistical errors, it also predicts the correct number of measured non-diffractive events. The 1.7σ discrepancy between simulation and data could be adjusted by modifying by about a factor of two the y -distribution of the leading particle at $y \simeq y_{max}$. In doing so, our simulation extrapolated losses ($\simeq 1\%$, see Table 2) change by much less than the 0.4% assigned systematic error.

References

- [1] The CERN-Pisa-Rome-Stony Brook Collaboration, “New Measurement of pp Total Cross Section at the CERN ISR”, Phys. Lett. 62B (1976) 460
- U. Amaldi et al., “Precision Measurement of pp Total Cross Section at the CERN ISR”, Nucl. Phys. B145 (1978) 367

- [2] M. Bozzo et al., The UA4 Collaboration, “Measurement of the Proton-Antiproton Total Cross Section at the CERN SPS Collider”, Phys. Lett. 147B (1984) 392
- [3] The CDF Collaboration , “Measurement of Small Angle Antiproton-Proton Elastic Scattering at $\sqrt{s} = 546$ and 1800 GeV”, Fermilab-Pub 93/232-E Submitted to Phys. Rev. D
- [4] The CDF Collaboration, “The CDF Detector: An Overview”, NIM A271 (1988) 387
The CDF Collaboration, “The CDF Vertex Time Projection Chamber System”, NIM A268 (1988) 75
- [5] The drift chambers of the FTF and FTB telescopes were built for the UA4 experiment. Construction details can be found in
F. Carbonara et al., “ A System of Two Dimensional Drift Chambers with Printed Board Cathode and Flat Solenoidal Delay Lines”, NIM 171 (1980) 479
- [6] N.A. Amos et al., The E-710 Collaboration, “A Luminosity Independent Measurement of the $\bar{p}p$ Total Cross Section at $\sqrt{s}=1.8$ TeV, Phys. Lett. B243 (1990) 158
- [7] The CDF Collaboration , “Measurement of $\bar{p}p$ Single Diffraction Dissociation at $\sqrt{s} = 546$ and 1800 GeV”, Fermilab-Pub 93/233-E Submitted to Phys. Rev. D
- [8] J.T. Carrol et al., “The CDF Level 3 Trigger”, NIM A300 (1991) 552
U. Joshi et al., “The Upgraded Level 3 Trigger for the CDF Experiment at the Fermilab Tevatron Collider”, Nucl. Phys. 23A (1991) 365

- [9] W. Galbraith et al., “Total Cross Sections of Protons, Antiprotons, π and K Mesons on Hydrogen and Deuterium in the Momentum Range 6-22 GeV/c”, Phys. Rev. 138B (1965) 913
- [10] S.P. Denisov, “Energy Dependence of π^- , K^- and \bar{p} Total Cross Sections on Protons in the Momentum Range up to 65 GeV/c”, Phys. Lett. 36B (1971) 528
- [11] A.S. Carrol et al., “Total Cross Sections of π^\pm , K^\pm , p and \bar{p} on Protons and Deuterons between 23 and 280 GeV/c”, Phys. Lett. 61B (1976) 303
A.S. Carrol et al., “Total Cross Sections of π^\pm , K^\pm , p and \bar{p} on Protons and Deuterons between 200 and 370 GeV/c”, Phys. Lett. 80B (1979) 423
- [12] N. Amos et al., “ Measurement of Small-Angle $p\bar{p}$ and pp Elastic Scattering at the CERN ISR”, Nucl. Phys. B262 (1985) 689
- [13] D.S. Ayres et al., “ π^\pm , K^\pm , pp and $p\bar{p}$ Elastic Scattering from 50 to 175 GeV/c”, Phys. Rev. D 15 (1977) 3107
- [14] G.J. Alner et al., The UA5 Collaboration, “Antiproton-proton Total Cross Sections at 200 and 900 GeV c.m. Energy”, Zeitschrift fuer Physik C32 (1986) 153
- [15] M. Ambrosio et al., “Measurement of the Elastic Scattering in $p\bar{p}$ Collisions at 52.8 GeV C.M. Energy”, Phys. Lett. 115B (1982) 495
- [16] N.M. Amos et al., “ Measurement of ρ , the Ratio of the Real to Imaginary Part of the $\bar{p}p$ Forward Elastic Scattering Amplitude, at $\sqrt{s}=1.8$ TeV”, Phys. Rev. Lett. 68 (1992) 2433

- [17] H. Cheng and T.T. Wu, "Limits of Cross Sections at Infinite Energy", Phys. Rev. Lett. 24 (1970) 1456
T.T. Chou and C.N. Yang, "Elastic Hadron-Hadron Scattering at Ultra High Energies and Existence of Many Dips", Phys. Rev. D19 (1979) 3268
- [18] R. Henzi and P. Vlain, "Towards a Blacker, Edgier and Larger Proton", Phys. Lett. 132B (1983) 444
- [19] R. Castaldi and G. Sanguinetti, " Elastic Scattering and Total Cross Sections at Very High Energies", Ann. Rev. Nucl. Part. Sci. (1985) 351
- [20] A. Donnachie and P.V. Landshoff, "Multi-Gluon Exchange in pp Elastic Scattering", Phys. Lett. 123B (1983) 345
P. Aurenche et al., "Multiparticle Production in a Two-Component Dual Parton Model", Phys. Rev. D45 (1992) 92
- [21] F. Abe et al., The CDF Collaboration, " Transverse Momentum Distribution of Charged Particles Produced in $\bar{p}p$ Interactions at $\sqrt{s}=630$ and 1800 GeV", Phys. Rev. Lett. 61 (1988) 1819
- [22] F. Abe et al., " Pseudorapidity Distribution of Charged Particles Produced in $\bar{p}p$ Interactions at $\sqrt{s}=630$ and 1800 GeV", Phys. Rev. D41 (1990) 2330
- [23] K. Goulianos, " A New Statistical Description of Hadronic and e^+e^- Multiplicity Distributions", Phys. Lett. B193 (1987) 151
- [24] G.J. Alner, The UA5 Collaboration, " Scaling of Pseudorapidity Distributions at C.M. Energies up to 0.9 TeV", Zeitschrift fuer Physik C33 (1986) 1

- [25] G.J. Alner, The UA5 Collaboration, "A General Study of Proton Proton Physics at $\sqrt{s}=546$ GeV, Phys. Rep. 154 (1987) 247
- [26] D.R. Ward, "Low p_t Physics at the $S\bar{p}pS$ Collider", Physics Simulations at High Energy, World Scientific (1986) 208

Table 1: Event flow through filters

	$\sqrt{s}=546$	1 st run at $\sqrt{s}=1800$	2 nd run at $\sqrt{s}=1800$
	Number of Events		
Triggers	45770	24123	205202
TOF FILTER	32252	6740	16605
VTPC FILTER	31717	5953	9638

Table 2: Corrections to the measured (W•E) inelastic rate

Loss corrections	$\sqrt{s}=546$	1 st run at $\sqrt{s}=1800$	2 nd run at $\sqrt{s}=1800$
TOF FILTER	1.000 ± 0.003	1.007 ± 0.001	1.007 ± 0.005
VTPC FILTER	1.005 ± 0.0007	1.0033 ± 0.0007	1.005 ± 0.002
Event-builder	1.100 ± 0.004	1.0	1.094 ± 0.004
MonteCarlo correction	1.016 ± 0.005	1.013 ± 0.004	1.013 ± 0.004
Prescaling factor	23.90 ± 0.10	11.43 ± 0.02	15.34 ± 0.02

Table 3: Vertex analysis event flow

Vertex by	$\sqrt{s}=546$		1 st run at $\sqrt{s}=1800$		2 nd run at $\sqrt{s}=1800$	
	all events	$\bar{p}p$ interactions	all	$\bar{p}p$	all	$\bar{p}p$
VTPC	28229	28229	5145	5079 \pm 84	8085	7834 \pm 92
Forward telescopes	3353	3353	679	435 \pm 56	1251	555 \pm 76
No vertex	135		129		302	
Total		31582 \pm 178		5514 \pm 93		8389 \pm 119

Table 4: Contributions of the various triggers to the corrected total number of events.

		$\sqrt{s}=546$	$\sqrt{s}=1800$
Inelastic (W•E)	1	847796 \pm 8302	208890 \pm 2558
Inel. (\bar{p} •E): single diffr.		162836 \pm 7986	37782 \pm 1770
Inel. (\bar{p} •E): single diffr. (*)	2	150151 \pm 7364	32092 \pm 1503
Inel. (\bar{p} •E): non-diffr.		24483 \pm 3926	10276 \pm 1712
Inel. (\bar{p} •E): non-diffr. (*)		2024 \pm 332	1311 \pm 222
Total inelastic (1+2)		997947 \pm 11097	240982 \pm 2967
Elastic		265535 \pm 2411	78691 \pm 1463
Total		1263482 \pm 11356	319673 \pm 3308
$dN_{el}/dt _{t=0}$ (events/GeV ²)		4043598 \pm 52915	1336532 \pm 40943

(*) after removal of events triggering also (W*E)

Table 5: Comparison of data with simulation for events collected by the (W•E) inelastic trigger

	Fraction of inelastic events (%)				
	$\sqrt{s} = 546$		$\sqrt{s} = 1800$		
Trigger by	sim	data	sim	data	data (*)
(BBCW•BBCE)•(S4+S5)	96.5	96.0	96.3	95.3	96.6
(S4•S5)•BBCE+(S4•S5)•BBCW	1.2	2.1	0.8	2.1	0.9
(S4•BBCE)+(S5•BBCW)	0.29	0.27	0.3	0.4	0.3
(S4•S5)	0.01	0.03	0.1	0.2	0.1
(BBCW•BBCE)	2.0	1.6	2.5	2.0	2.1
No vertex	0.4	0.4	0.1	2.3	
θ_{max} -track in the					
VTPC	95.2	94.1	96.3	91.7	96.5
FTF+FTB	4.2	5.2	3.5	5.5	3.4
S4+S5	0.2	0.3	0.1	0.5	0.1

(*) after background subtraction

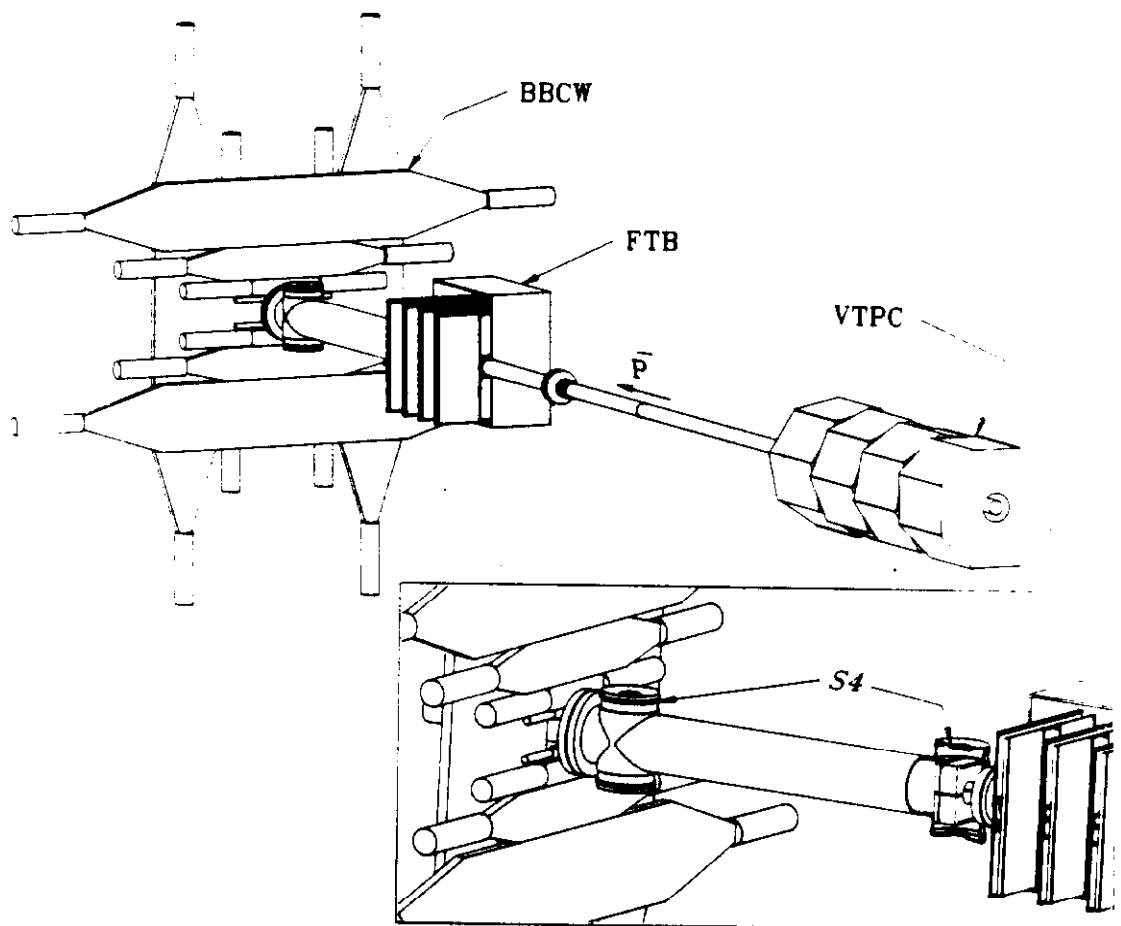


Figure 1: Layout of the west side (outgoing \bar{p}) of the apparatus used to measure the inelastic cross section (the detector is symmetric with respect to the interaction point). An exploded view of the S4 detector is also shown.

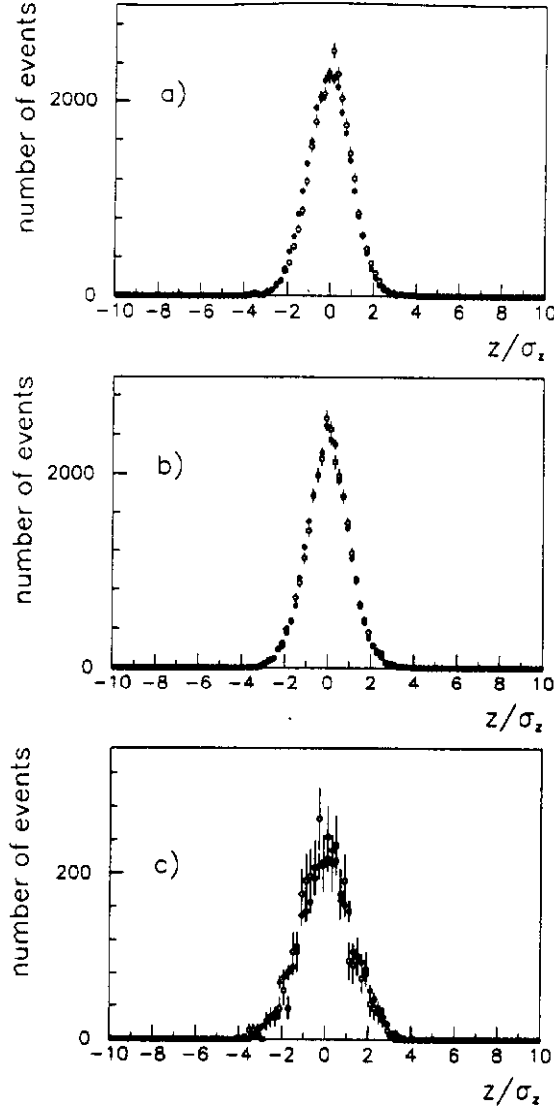


Figure 2: Vertex z -distributions measured at $\sqrt{s}=546$ GeV for (•) data that passed all cuts listed in Table 1, and (○) simulated inelastic events reconstructed as the data and normalized to the number of measured events.

(a) Vertex measured by the VTPC in units of the spread σ_z ($\simeq \pm 30$ cm) of the interaction region. The vertex reconstruction accuracy of the VTPC is $\simeq \pm 1$ cm.

(b) Vertex measured by the forward telescopes for the events in (a). In this case, σ_z is the convolution of the spread of the interaction with the reconstruction error for each vertex ($\simeq \pm 6$ cm).

(c) Vertex measured by the forward telescopes for events without a VTPC vertex. Here σ_z is defined as in (b). The z -distribution widths of the data and simulation are larger than in (b) because of the increasing importance of secondary interactions in the beam pipe in events with only forward prongs.

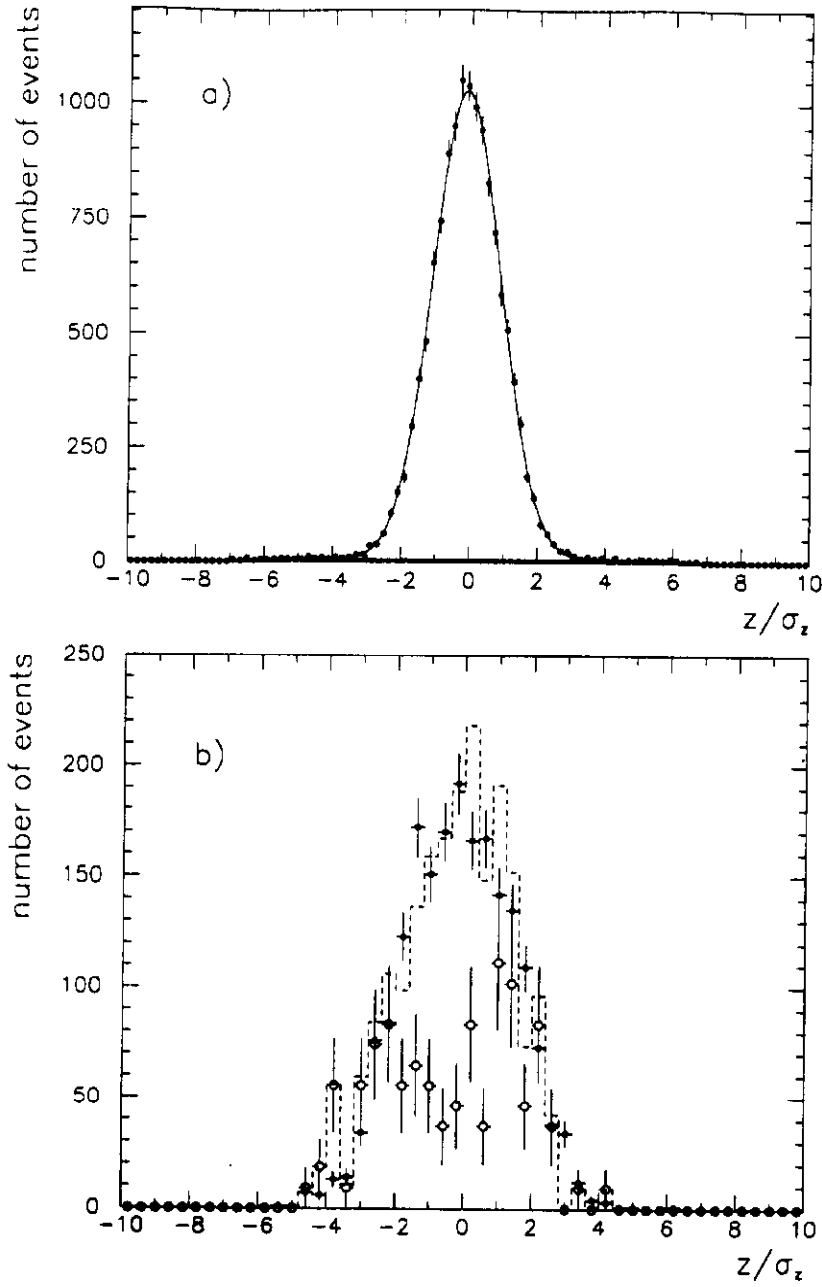


Figure 3: Vertex z -distributions at $\sqrt{s}=1800$ GeV.

(a) Vertex measured by the VTPC; $\bar{p}p$ interactions were evaluated by fitting to the data a gaussian of width as determined by the simulation, and a flat background.

(b) Vertex z -distribution measured by the forward telescopes for events without a VTPC vertex. The data (•) were fitted with a gaussian of width as determined by the simulation and a background contamination, the shape of which was determined from tagged background events (◊); the dashed line represents the fit result.

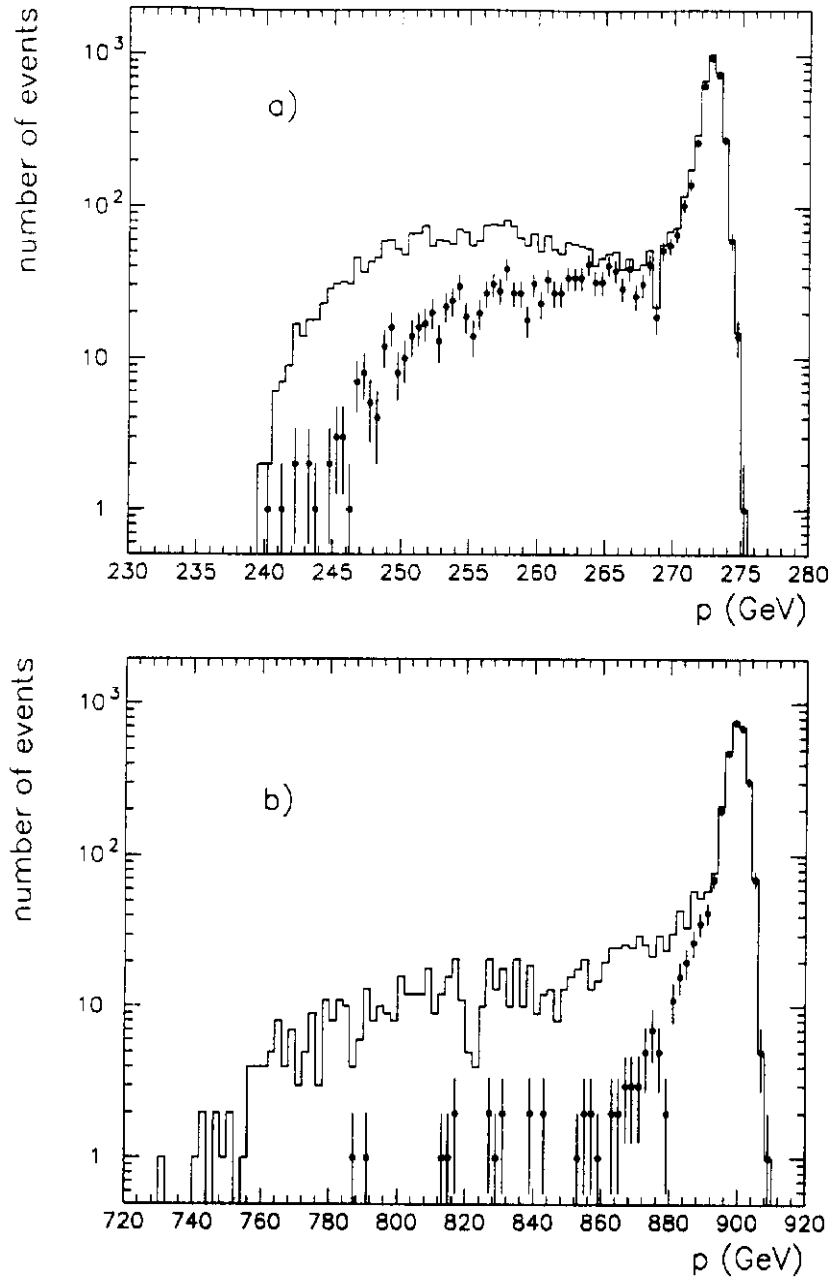


Figure 4: (a) Momentum distribution of the diffractive recoil antiproton at $\sqrt{s}=546$ GeV: (solid line) all events accepted by the single diffraction trigger ($\bar{p} \bullet E$); (\bullet) events which did not fire the inelastic trigger ($W \bullet E$).
(b) Similar momentum distribution at $\sqrt{s}=1800$ GeV.

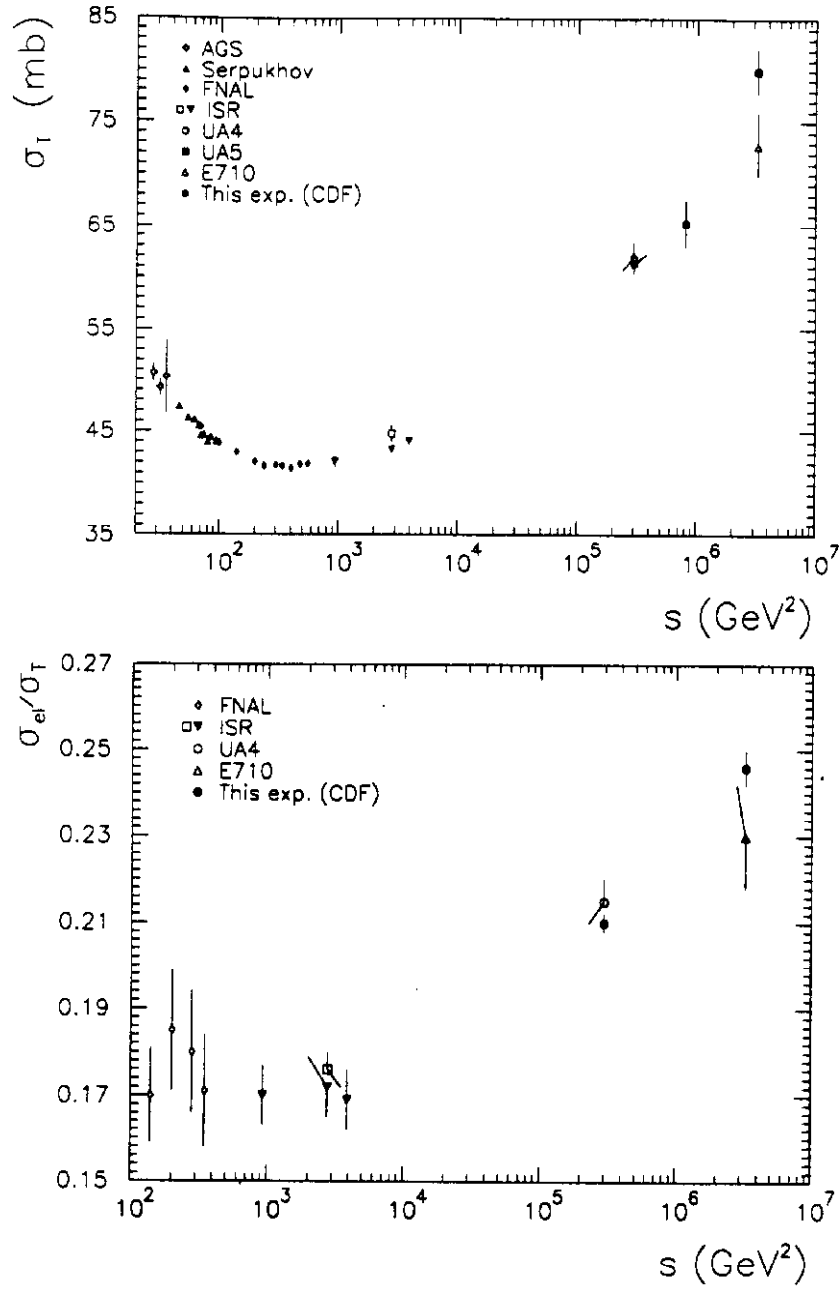


Figure 5: Results of this experiment shown together with other $\bar{p}p$ measurements.
(a) Total cross section : AGS Ref.[9], Serpukhov Ref.[10], FNAL Ref.[11], ISR Ref.[12, 15], UA4 Ref.[2], UA5 Ref.[14], E710 Ref.[16].
(b) The ratio σ_{el}/σ_T : FNAL Ref.[11, 13], ISR Ref.[12, 15], UA4 Ref.[2], E710 Ref.[6]

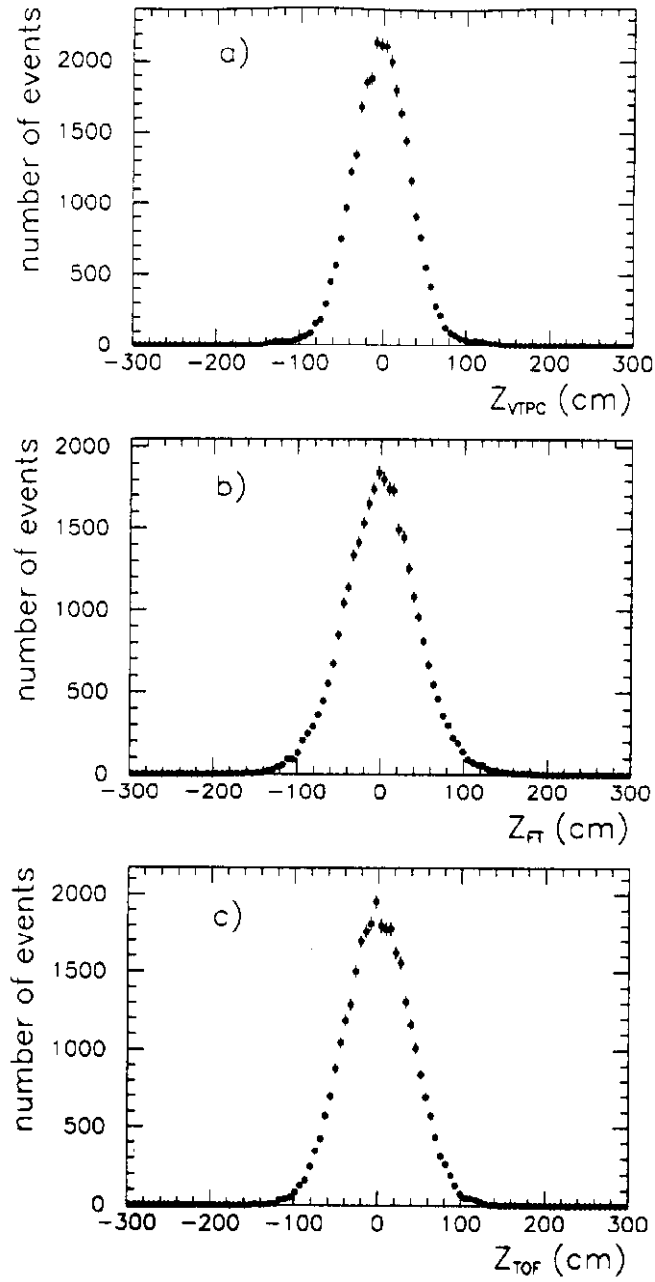


Figure 6: Vertex z -distributions as measured by (a) the VTPC, (b) the forward telescopes and (c) the timing information of the trigger counters in all events at $\sqrt{s}=546$ GeV.

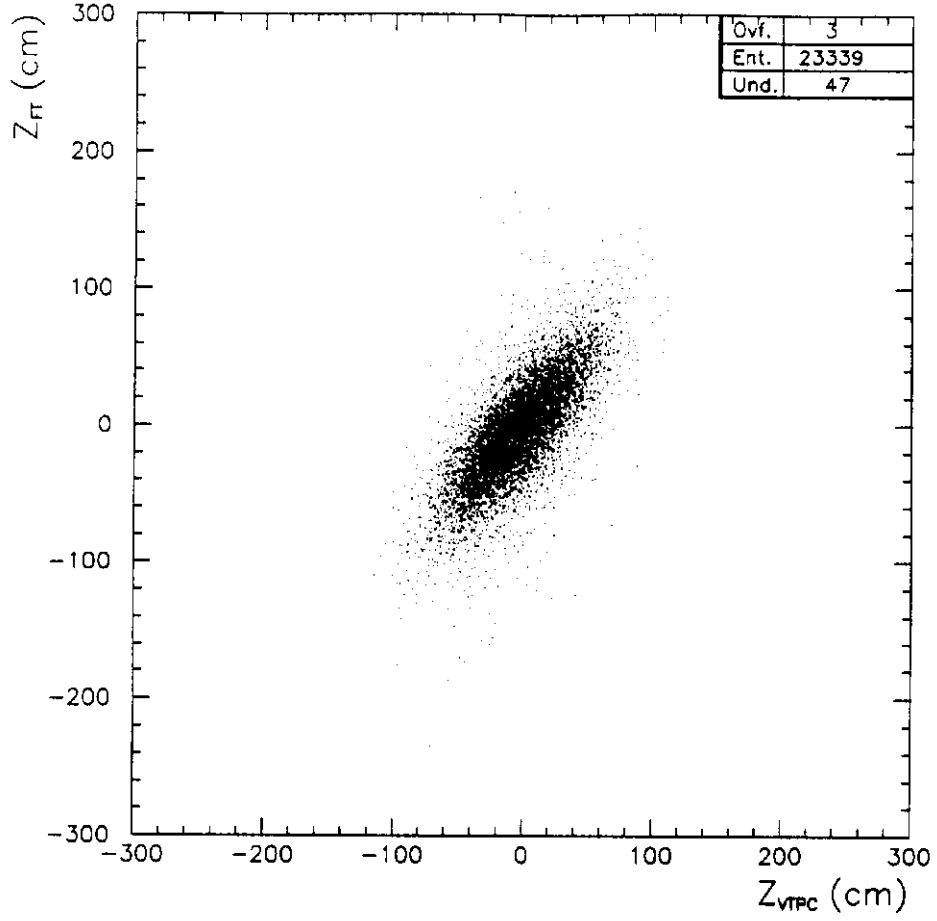


Figure 7: Vertex z -position determined by the forward telescopes vs. the vertex z -value measured by the VTPC. At $\sqrt{s}=546$ GeV, the forward telescopes reconstructed 99.8 % of the events seen by the VTPC.

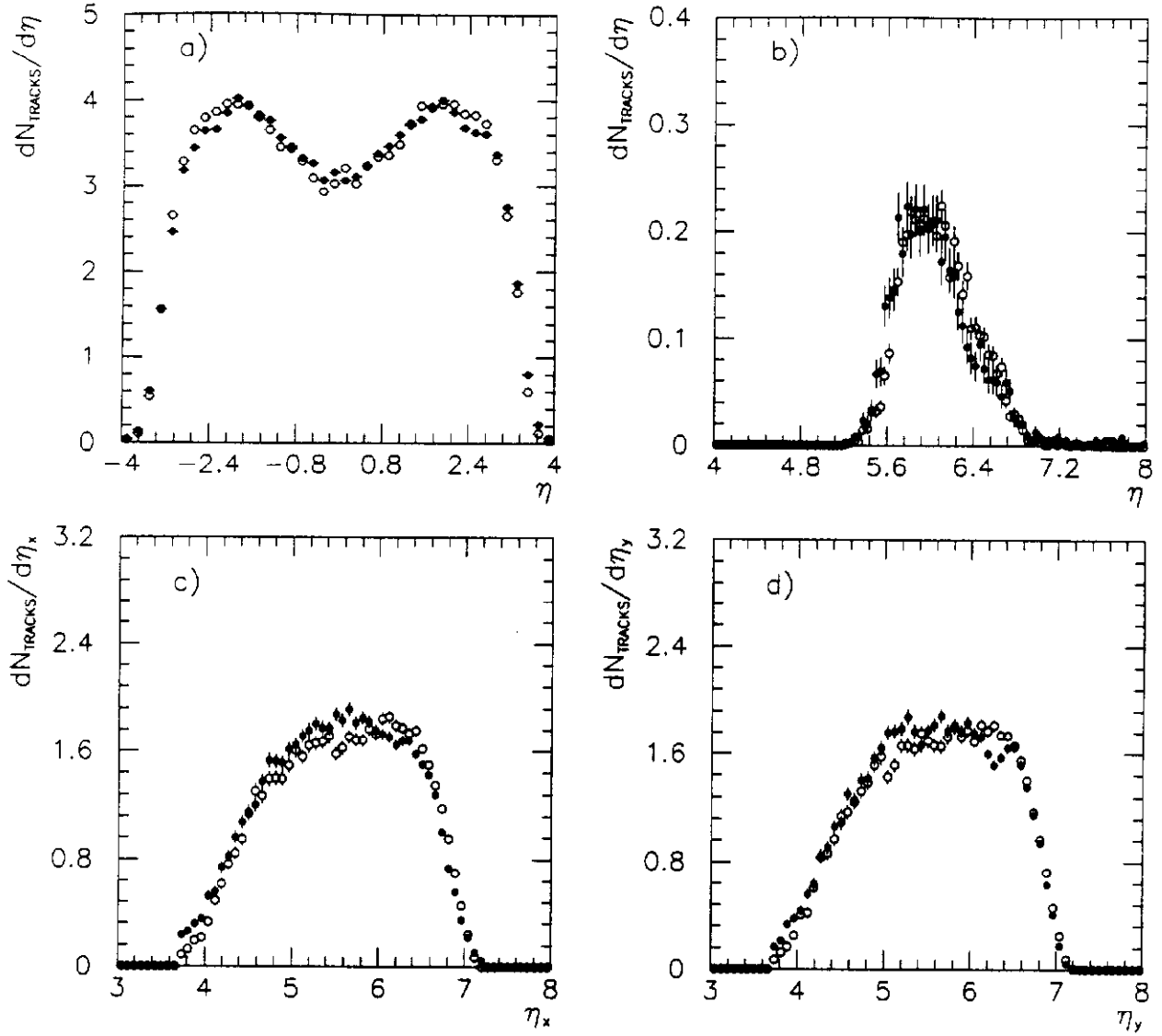


Figure 8: Pseudo-rapidity distributions as measured by the different vertex detectors at $\sqrt{s} = 546$ GeV. The data (\bullet) are not corrected for detector acceptance. The simulation (\circ) is normalized to the total number of measured tracks.

(a) η -distribution of tracks detected by the VTPC.

(b) $|\eta|$ -distribution measured by S4+S5.

(c,d) $|\eta_x|$ and $|\eta_y|$ -distributions measured by the FTF+FTB. The angles θ_x and θ_y are measured independently; $\eta_{x(y)} = -\ln(\tan \frac{\theta_{x(y)}}{2})$.

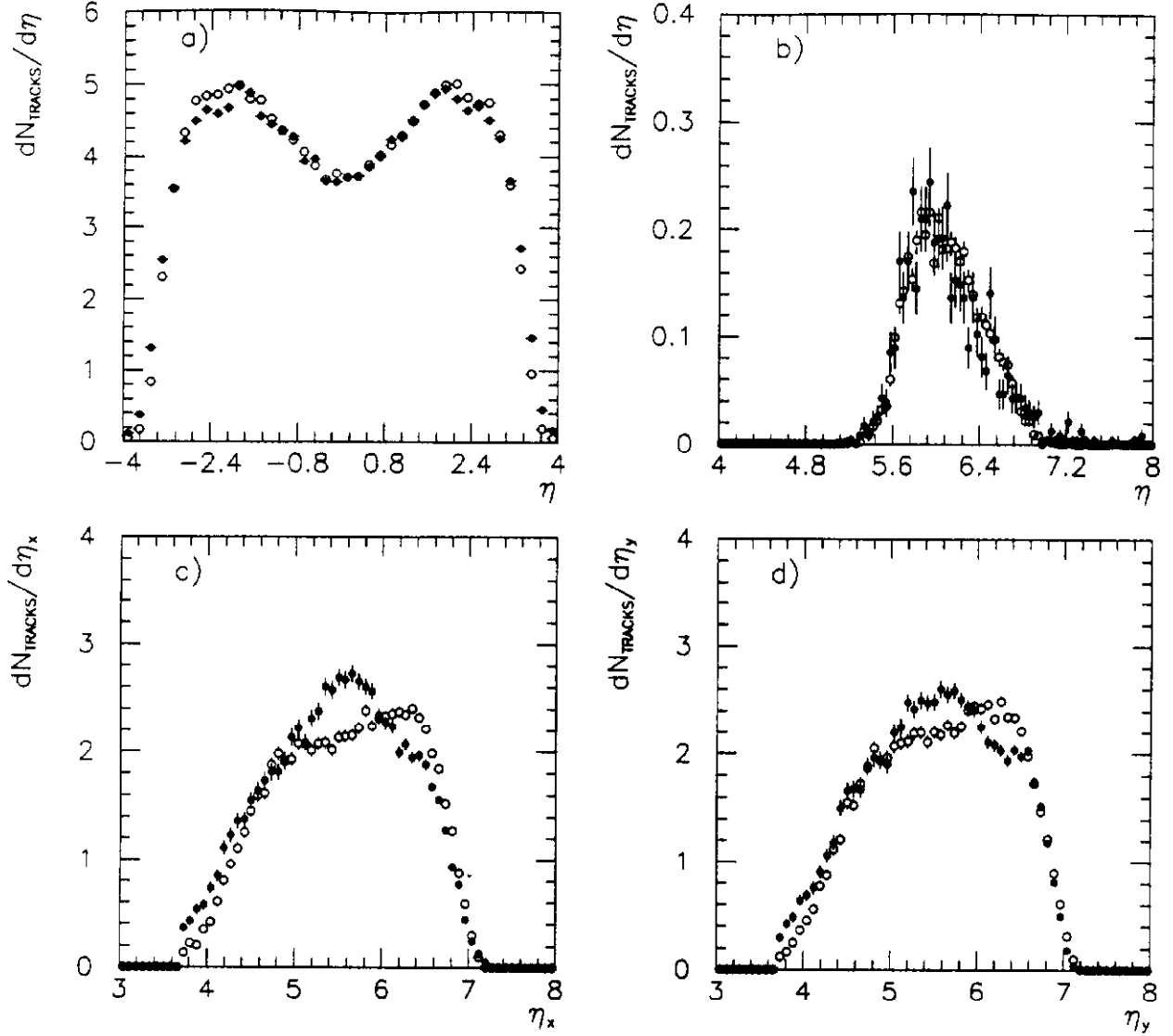


Figure 9: Pseudo-rapidity distributions as measured by the different vertex detectors at $\sqrt{s} = 1800$ GeV. The data (\bullet) are not corrected for the detector acceptance. The background ($\approx 1\%$ in the VTPC and $\approx 35\%$ in the forward telescopes) has not been removed. The simulation (\circ) is normalized to the total number of measured tracks for every detector.

(a) η -distribution of tracks detected by the VTPC.

(b) $|\eta|$ -distribution measured by S4+S5.

(c,d) $|\eta_x|$ and $|\eta_y|$ -distributions measured by the FTF+FTB.

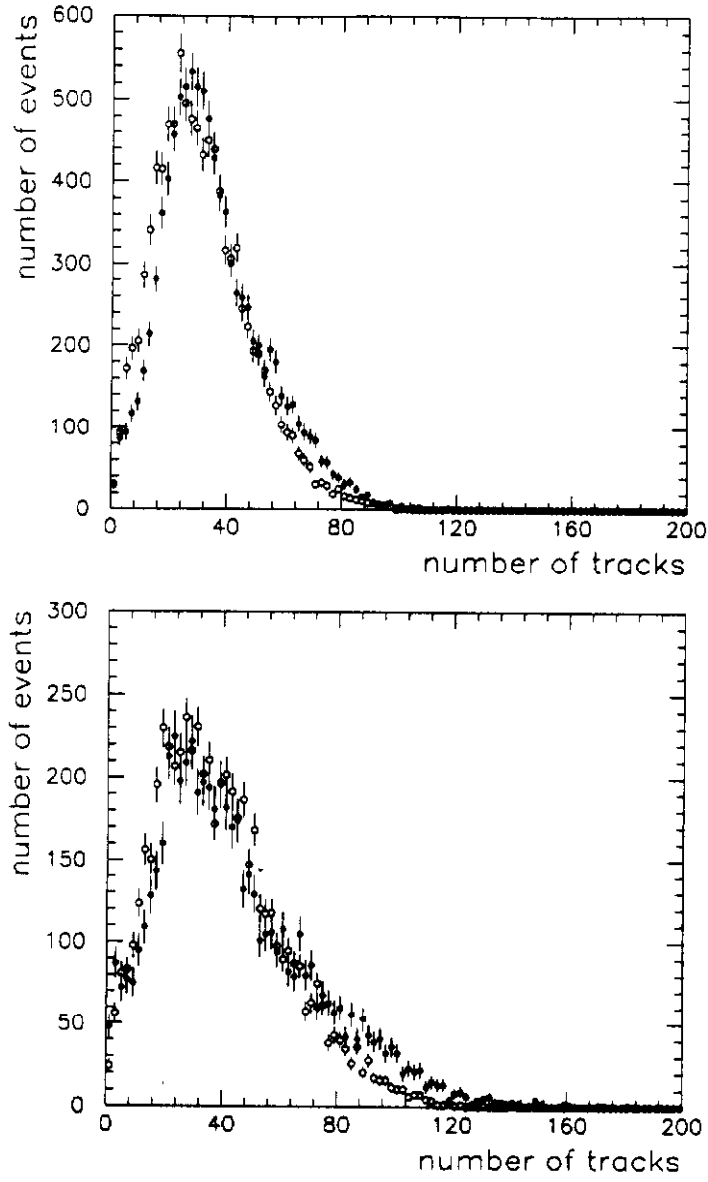


Figure 10: Multiplicity distribution of tracks measured in all detectors. Data (\bullet) and simulation (\circ) are compared at (a) $\sqrt{s}=546$ and (b) $\sqrt{s}=1800$ GeV.

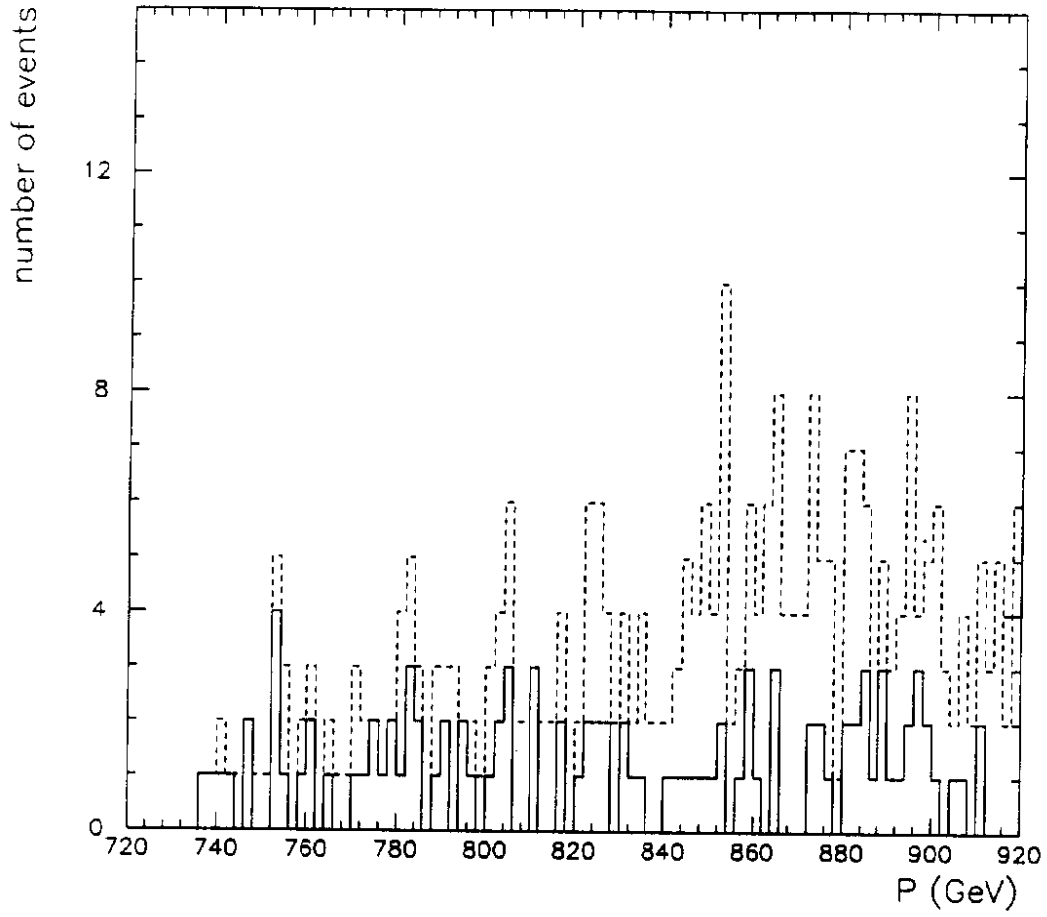


Figure 11: Momentum distribution of particles detected by the single diffraction recoil spectrometer in 70400 simulated inelastic events, before (dashed line) and after (solid line) applying the fiducial cuts described in Ref. [7].